Absolute fluorescence and absorption measurements over a dynamic range of 10^6 with cavity-enhanced laser-induced fluorescence

Scott E. Sanders,[1, a)] Oliver R. Willis,[1, b)] N. Hendrik Nahler,[2] and Eckart Wrede[1, c)]

[1)] *Department of Chemistry, Durham University, Durham DH1 3LE, United Kingdom*

[2)] *School of Engineering and Physical Sciences, Heriot-Watt University, Edinburgh EH14 4AS, United Kingdom*

We present a novel spectroscopic technique that exhibits high sensitivity and a large dynamic range for the measurement of absolute absorption coefficients. We perform a simultaneous and correlated laser-induced fluorescence and cavity ring-down measurement of the same sample in a single, pulsed laser beam. The combined measurement offers a large dynamic range and a lower limit of detection than either technique on its own. The methodology, dubbed cavity-enhanced laser-induced fluorescence (CELIF), is developed and rigorously tested against the electronic spectroscopy of 1,4-bis(phenylethynyl)benzene in a molecular beam and density measurements in a cell. We outline how the method can be used to determine absolute quantities, such as sample densities, absorption cross sections and fluorescence quantum yields, particularly in spatially confined samples.

Keywords: molecular spectroscopy, laser-induced fluorescence, cavity ring-down spectroscopy, fluorescence quantum yield.

I. INTRODUCTION

Laser-induced fluorescence (LIF) is a spectroscopic method widely used because of its extreme sensitivity.[1–3] However, as an indirect absorption measurement, LIF is often unsuitable for analytical purposes and the determination of absolute quantities. Cavity ring-down spectroscopy (CRDS), on the other hand, is a direct absorption technique and therefore provides an absolute measurement but generally possesses a lower sensitivity, in particular for spatially confined samples. Here, we present a novel, direct combination of laser-induced fluorescence with cavity ring-down spectroscopy that allows the measurement of absolute absorption coefficients several orders of magnitude below the limit of detection of pulsed UV/vis CRDS with a much increased dynamic range. We name this combination cavity-enhanced laser-induced fluorescence, CELIF.

Laser-induced fluorescence forms the main part of a CELIF measurement. Fluorescence follows the electronic excitation of a species upon absorption of UV/vis laser light. Most commonly, the wavelength-integrated fluorescence is detected leading to a fluorescence excitation spectrum that is directly linked to the absorption spectrum by the fluorescence quantum yield. Additional in-formation can be obtained from the wavelength-dispersed fluorescence. In general, LIF possesses intrinsically low noise allowing the detection of very low concentrations in confined volumes.

An absolute measurement of absorbance requires detailed knowledge of the fluorescence process and meticulous calibration of the detection system (fluorescence quantum yield, geometrical setup, spectral response of the detector, *etc.*). Because of the calibration challenges, LIF is predominantly used to measure relative rather than absolute quantities. Generally, laser-induced fluorescence is measured with amplified photodetectors. These detectors possess maximum gains of 10^6 to 10^8 which allow the measurement of the fluorescence signal over a large dynamic range. The measurement is virtually background free if stray light from the incident laser is suppressed effectively, *e.g.* with an optical filter. If the fluorescence lifetime exceeds the time between collisions, quenching of the fluorescence can occur, reducing the signal potentially to a level which makes a measurement impossible. In addition, quenching, predissociation and other non-radiative processes complicate a straightforward relationship between signal and concentration, due to possible dependences of these processes on the excited state. Nevertheless, LIF measurements have been carried out in different media from collision-free environments, *e.g.* molecular beams, to liquids and solids.[4]

Over the last two decades, cavity ring-down spectroscopy (CRDS) has become a well-established and widely-applied spectroscopic technique.[5–7] A conventional cav-

---

a)Current address: AWE, Aldermaston, Reading, RG7 4PR, U.K.
b)Current address: CPI, NETPark, Sedgefield, TS21 3FG, U.K.
c)Electronic mail: eckart.wrede@durham.ac.uk

ity ring-down (CRD) measurement is based on the Beer-Lambert law and performs a direct absorption measurement. Consequently, fluorescence of the sample is not a detection requirement. In a CRD experiment, light enters a cavity formed by two highly reflective mirrors (typically $R > 0.999$). During each pass a small fraction of light leaks out through the mirrors and is detected as an exponential decay behind the exit mirror. The inverse of the decay rate is referred to as ring-down time, which for an empty cavity is given by[7]

$$\tau_0 = \frac{d}{c(1-R)}, \tag{1}$$

where d is the distance between the mirrors of reflectivity R and c is the speed of light. Depending on the reflectivity of the mirrors, several thousand round trips can be achieved. For typical values of $R = 0.999$ and $d = 1$ m the effective path length is 1 km. The absorption of light by a sample inside the cavity causes an additional loss and consequently a shorter ring-down time. For a filled cavity, the reduced ring-down time, τ, is directly linked to the absorption coefficient

$$\alpha = \sigma\rho = \frac{1}{c}\left(\frac{1}{\tau} - \frac{1}{\tau_0}\right), \tag{2}$$

where σ is the absorption cross section and ρ is the number density of the sample leading to a fractional absorption per pass of $\mathcal{L} = \alpha d$. As the ring-down time is measured, the technique is immune to power fluctuations of the incident laser, leading to a high sensitivity in comparison to most other absorption techniques. In contrast to LIF, absolute absorption coefficients can be directly obtained by measuring the ring-down times with and without the sample.

In cavity ring-down spectroscopy, the absorbance is measured over the path length through the sample (integrated column density) and, unlike LIF, is not spatially resolved. Similar to LIF, CRDS has been applied to gas-phase, liquid and solid samples.[8–10] A CRDS measurement is based on the detection of a small change in signal on a large background and its dynamic range is restricted by the minimal and maximal detectable change in ring-down time. Historically, CRDS was developed as a pulsed technique in the visible spectral region probing electronic transitions. Such setups typically span a dynamic range of three orders of magnitude.[11] More recent advances in infra-red optics and light sources led to the development of more and more sensitive cavity-enhanced spectroscopic techniques that probe vibrational overtone transitions using cw IR light.[12] The limit of detection of LIF is generally superior for a spatially confined sample whereas CRDS can exceed this limit if the sample fills the entire length of the cavity.

CELIF is a direct combination of LIF and CRDS that employs a single, pulsed laser beam inside the optical cavity interacting with the same sample for both the fluorescence and ring-down measurements. The transients from the LIF and CRD detectors are recorded simultaneously on a shot-to-shot basis. For the first time, the analysis of both transients is correlated such that the detected fluorescence is normalized to compensate for fluctuating laser intensities which are obtained from the time-integrated ring-down transient. A simultaneous ring-down time measurement provides the robust calibration of the background-free but otherwise indirect fluorescence measurement.

Previously, several groups have used different combinations of LIF and CRD, not necessarily using a single laser beam, to measure, *e.g.*, fluorescence quantum yields and quenching rates.[13–16] Richman *et al.* detected fluorophor-doped aerosols within a cavity by their fluorescence signal.[17] Furthermore, CRD spectroscopy, instead of Rayleigh scattering, has recently been used to calibrate density measurements in flames via LIF.[18–20] None of these previous studies used the correlation of the LIF and CRD measurements as presented here.

In this paper, we develop the CELIF methodology based on the simultaneous LIF and CRD measurements. We present experimental results that scrutinize the methodology, particularly the increased dynamic range and the significantly lower limit of detection in comparison to the standalone CRDS setup.

II. EXPERIMENT

The fundamental idea of CELIF is to measure the fluorescence of a sample situated inside a traditional ring-down cavity simultaneously with the ring-down decay. A schematic layout of the setup is shown in Fig. 1. It is a straightforward combination of a classical LIF and pulsed CRDS setup: the sample is intersected by the laser beam that is confined in the cavity and the laser-induced fluorescence is collected at right angles. In our setup the
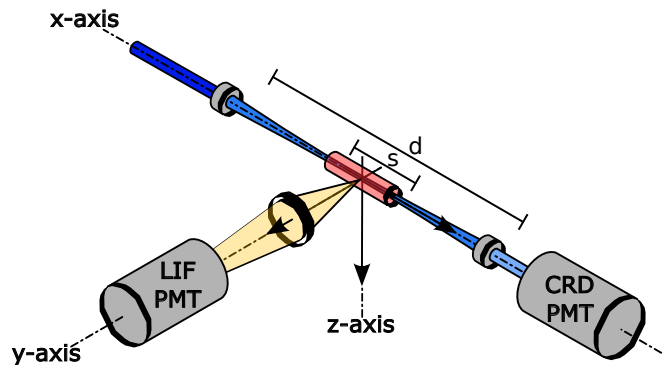
FIG. 1. Experimental setup. The sample volume is situated at the center of the ring-down cavity (x-axis) and the fluorescence is collected at right angles (y-axis). d is the distance between the mirrors and s the length of the sample.

wavelength-integrated fluorescence is recorded. Without loss of generality, the technique can be used in a setup where the dispersed fluorescence spectrum is measured. In principle, the technique should be widely applicable to any gas-phase, liquid and even solid samples which have been used in previous CRDS studies as long as the fluorescence light can be extracted from the sample volume.

A. CELIF method

In a CELIF measurement, the following three quantities are extracted from the simultaneously recorded CRD and LIF transients: the ring-down time, τ, the time-integrated ring-down transient, S^{CRD}, and the time-integrated fluorescence transient, S^{LIF}. The latter two are a measure of the amount of light incident on the respective detectors. In the following, we derive how these three quantities are used to normalize and to calibrate the LIF measurement to determine absolute absorption coefficients.

In a general LIF measurement, the detected fluorescence, S^{LIF}, is proportional to the light intensity, I_{L}, that has interacted with the sample within the LIF probe volume:

$$S^{\mathrm{LIF}}(\lambda) = \alpha(\lambda) \cdot \Gamma(\lambda) \cdot g \cdot I_{\mathrm{L}} \,, \qquad (3)$$

where λ is the excitation wavelength, Γ is the fluorescence quantum yield and g is a geometry dependent factor of the detection system. In principle, g is also a function of λ as the fluorescence spectrum may depend on the excited state. However, this dependence can only be considered if the dispersed fluorescence spectrum is recorded as a function of excitation wavelength. In order to obtain the absorption coefficient, α, from a fluorescence excitation measurement, S^{LIF} and I_{L} need to be measured. The factor g is an instrument function that is not readily available but can be determined via a meticulous external calibration. The fluorescence quantum yield, Γ, is generally unknown and needs to be measured or predicted from theory in a separate study.[21]

In the following, we show how the time-integrated CRD transient, S^{CRD}, is correlated to I_{L} and how it is subsequently used to provide the normalization of S^{LIF} to eliminate shot-to-shot fluctuations in the laser intensity from Eq. 3. We then describe how the absolute absorption coefficient determined from the ring-down time (Eq. 2) is used for the absolute calibration of the normalized LIF measurement such that in a CELIF measurement prior knowledge of g and Γ is not required.

However, there are differences in the measurement of the fluorescence between a CELIF and a typical single-pass LIF experiment. The entrance mirror of the ring-down cavity rejects the majority of the laser pulse and, as a consequence, the initial fluorescence is very weak in comparison to single-pass LIF. CELIF greatly reduces satura-

tion and power broadening due to the much lower photon densities and, for a transversally mode-matched cavity,[22] effectively eliminates stray light. As in any cavity ring-down setup, the cavity acts as a spatial and as a frequency filter. The coupling of the frequency spectrum of the laser into the cavity modes has been discussed extensively in the cavity ring-down literature.[23–26] Similar to a cavity ring-down setup, a user of CELIF must consider the spectral properties of both laser and cavity and the absorption of the sample in the experimental design and data analysis.[25] The normalization and calibration of the CELIF signal is independent of the spectral composition of the light as both the LIF and CRD measurements are based on the same photons interacting with the sample. Therefore, the following derivation uses the photon-bullet model,[6] i.e. we only consider the time-dependence of the recorded transients.

As in any CRD setup, the laser pulse decays exponentially leading to an increased interaction time with the sample. The pulse confined in the cavity undergoes up to several thousand round trips, interacting with the sample twice on each of them. Each of these interactions induces further fluorescence such that the total fluorescence detected leads to an appreciable integrated LIF transient. Without loss of generality, we assume a sample distribution that is symmetric with respect to a LIF probe volume that is placed at the center of the cavity. The fractional absorption per pass is $\mathcal{L} = \alpha s$, with the sample length, s, given that $\mathcal{L} \ll 1$. The light intensity at the center after entering the cavity is

$$I_0 = I_{\mathrm{in}} T \left(1 - \frac{\mathcal{L}}{2} \right) \,, \qquad (4)$$

where I_{in} is the laser intensity incident on the cavity entrance mirror and T is the (intensity) transmission of the mirror. In the following derivation we assume identical cavity mirrors. In addition to the sample loss, a fraction of light leaks out of the cavity upon reflection at the mirror. The light intensity at the center of the cavity after i single passes is

$$I_i = I_0 \left[(1 - \mathcal{L}) R \right]^i \,, \qquad (5)$$

where R is the (intensity) reflectivity of the cavity mirrors. Using the summation rule for geometric series, the summed light intensity, I_n, that has crossed the LIF probe volume after n single passes and the integrated intensity in the limit $n \to \infty$, I_{L}, are:

$$I_n = I_0 \sum_{i=0}^{n} \left[(1 - \mathcal{L}) R \right]^i = I_0 \frac{1 - \left[(1 - \mathcal{L}) R \right]^{n+1}}{1 - (1 - \mathcal{L}) R} \,, \qquad (6)$$

$$I_{\mathrm{L}} = \lim_{n \to \infty} I_n = \frac{I_0}{1 - (1 - \mathcal{L}) R} \,. \qquad (7)$$

Using Eq. 4 and the approximations $\mathcal{L} \ll 1$ and $T \approx 1 - R$ shows that $I_{\mathrm{L}} \approx I_{\mathrm{in}}$. This means that, through the repeated use of the decaying light pulse inside the

cavity, the amount of light that interacts with the sample is approximately the amount incident on the entrance mirror.

Similarly, we can correlate the integrated CRD transient, S^{CRD}, to the light incident on the cavity entrance mirror, I_{in}. The transient is measured at the exit mirror taking into account that, following the initial single pass (I_0^{CRD}), light is only collected after every round trip:

$$I_0^{\mathrm{CRD}} = I_{\mathrm{in}} T^2 (1 - \mathcal{L}), \tag{8}$$

$$I_n^{\mathrm{CRD}} = I_0^{\mathrm{CRD}} \sum_{j=0}^{n/2} [(1 - \mathcal{L}) R]^{2j}$$

$$= I_0^{\mathrm{CRD}} \frac{1 - \left[(1 - \mathcal{L})^2 R^2\right]^{n+1}}{1 - (1 - \mathcal{L})^2 R^2}, \tag{9}$$

$$S^{\mathrm{CRD}} = \lim_{n \to \infty} I_n^{\mathrm{CRD}} = \frac{I_0^{\mathrm{CRD}}}{1 - (1 - \mathcal{L})^2 R^2}. \tag{10}$$

In the limit of an empty cavity ($\mathcal{L} = 0$) and $T = 1 - R \ll 1$, the measured, time-integrated light intensity incident on the CRD detector is

$$S^{\mathrm{CRD}} = I_{\mathrm{in}} T/2. \tag{11}$$

The integrated light intensity interacting with the sample, I_{L}, and S^{CRD} are linked through Eqs 4, 7, 8 and 10:

$$I_{\mathrm{L}} = S^{\mathrm{CRD}} \frac{[1 + (1 - \mathcal{L})R](1 - \mathcal{L}/2)}{T(1 - \mathcal{L})}. \tag{12}$$

In the limit of $\mathcal{L} \ll 1$ and additionally $R \approx 1$, I_{L} can be approximated as

$$I_{\mathrm{L}} \approx S^{\mathrm{CRD}} \frac{1 + R}{T} \approx S^{\mathrm{CRD}} \frac{2}{T}. \tag{13}$$

As an example, for a relatively poor mirror reflectivity of $R = 0.998$ and a large fractional absorption of $\mathcal{L} = 0.001$, which would be amenable to a single-pass absorption measurement, the relative error of this approximation is smaller than 10^{-3}. This error is dominated by the mirror reflectivity and reduces to $5 \cdot 10^{-5}$ for $R = 0.9999$.

Therefore, we define the normalized CELIF signal by combining Eqs 3 and 13 as

$$S^{\mathrm{CELIF}} = \frac{S^{\mathrm{LIF}}}{S^{\mathrm{CRD}}} = \alpha \cdot \mathcal{K}, \tag{14}$$

where, in the photon-bullet model, $\mathcal{K} = 2 \cdot \Gamma \cdot g/T$. Note that S^{CELIF} is a relative quantity (unitless in our case) proportional to the absorption coefficient, α. The generally unknown proportionality factor $\mathcal{K}$ can be obtained through an internal calibration based on a simultaneous ring-down time measurement, provided the absorption leads to a sufficient reduction in ring-down time, $\Delta\tau = \tau_0 - \tau$:

$$\mathcal{K} = c \frac{\tau_0 \cdot \tau}{\Delta\tau} \cdot \frac{S^{\mathrm{LIF}}}{S^{\mathrm{CRD}}}. \tag{15}$$

This calibration is particularly robust as both the LIF and CRD measurements use the same photons to excite the same sample.

Note that $\mathcal{K}$ depends on the experimental parameters of the detection system, and the gains of both the LIF and the CRD detectors in particular, thus, the calibration needs to be repeated after any change of detection parameters. Equations 14 and 15 hold true for an absorption measurement at a fixed wavelength. Generally, $\mathcal{K}$ is a function of the excitation wavelength (fluorescence quantum yield, exit mirror transmission, mirror reflectivity) and the fluorescence spectrum (spectral response of the detection system). A single-pass LIF measurement needs to account for the wavelength dependencies of the quantum yield and the detection system in the same way. In Sec. IV A we describe a procedure that uses the simultaneously measured ring-down times and Rayleigh scattering collected with the LIF detection setup to determine the wavelength dependence of T based on our unchanged setup. With two sets of UV and visible mirrors we found the transmission to vary by less than 5% over a wavelength range of 1 nm, which will allow the approximation of the transmission as constant in many applications. We note, however, that the common approximation $T = 1 - R$, with $R(\lambda)$ derived from an empty-cavity ring-down scan, could not be generally applied over the usable wavelength range of each set of mirrors.

The derivation above is based on the photon-bullet model that ignores the phase and spectral dependencies of the cavity and laser fields. However, both S^{CRD} and S^{LIF} are identically affected by the spectral properties of the light interacting with sample. Hence, Eqs 14 and 15 are generally applicable to arbitrary input light fields.

Without loss of generality, we assumed the LIF measurement to be background-free (see Eqs 3 and 14), i.e. for an empty (sample-free) cavity the LIF signal is zero. However, this is rarely true in practice and we discuss the extraction of background-subtracted absorption coefficients in the supplementary material.

In the derivation above, Eqs 2–15, we have assumed an even sample distribution throughout the cavity, which is the case in a typical cell experiment. However, for localized samples, e.g. when using molecular beams, the sample density is not uniform. Both CRDS and LIF measure an average sample density (or absorption coefficient) over their respective probe volumes, cf. Eqs 2 and 3. Knowledge of the sample distribution is required in order to obtain the correct absorption coefficient of the sample.

B. Apparatus

A general CELIF setup is shown in Fig. 1. It consists of a basic ring-down cavity including beam-shaping, mode-

matching optics and a suitably fast photodetector (x-axis in figure). A typical LIF detection system, including a collimation lens and photodetector, is added at right angles to the cavity axis, preferably at the center of the sample (y-axis in figure). Two experimental setups were used in this study. Setup 1 introduced the sample via an unskimmed molecular beam (z-axis in figure) whereas Setup 2 was used for cell measurements where the entire cavity was filled with the sample gas.

Setup 1 was based on our CRD spectrometer that was used to study the torsional motions of jet-cooled 1,4-bis(phenylethynyl)benzene (BPEB), the details of which are described in Ref. 27. Briefly, solid BPEB was sublimated in a heated oven attached to the front of a pulsed solenoid valve (Parker, General Valve Series 9). The gaseous BPEB was picked-up by the argon carrier gas in the channel of the oven and cooled in the subsequent supersonic expansion. The relative BPEB sample density could be controlled over more than three orders of magnitude by varying the oven temperature. With a beam divergence of $\approx 20°$ (FWHM) the effective sample length is about 2 mm.[27] The cavity axis crossed the molecular beam approximately 5 mm downstream of the oven orifice. The $S_1 \leftarrow S_0$ transition of BPEB is very strong[28,29] and was excited over a wavelength range of 317–321.5 nm. Over this range, the reflectivity of the cavity mirrors (Layertec, center wavelength 330 nm) varied from 99.8 to 99.9% leading to empty-cavity ring-down times of $1.2 - 2.5$ μs (cavity length $d = 84$ cm). The doubled output of the dye laser (Sirah Cobra-Stretch, pumped by Continuum Surelite I-10, 10 Hz repetition rate) ranged from 30 to 100 μJ with a bandwidth of ≈ 0.05 cm^{-1} and a pulse length of ≈ 5 ns. The LIF collection optics imaged the full probe volume (overlap of molecular and laser beams) onto the photodetector.

With Setup 2, we carried out N_2 Rayleigh scattering (at 583.5 nm) and acetone fluorescence (at 313 nm) measurements to verify the methodology as described in Sec. II A. We note that the same detector setup was used for the Rayleigh scattering and fluorescence measurements. We use the term CELIF signal irrespective of light originating from a fluorescence or scattering event. In both cases the same measurement and analysis procedure are carried out. The gas pressure of the filled cavity (length $d = 81$ cm) was monitored over a range of $0.01 - 1000$ mbar with capacitance manometers (Leybold CR090/CTR100 and MKS 626A) to cross-reference the spectroscopically determined sample densities. For the Rayleigh scattering measurements, empty-cavity ring-down times in excess of 40 μs were achieved with the corresponding set of mirrors ($R > 99.99\%$). For the fluorescence measurements, the same set of mirrors was used as in Setup 1 and the drop-off in their reflectivity to about 99.7% shortened the ring-down time to ≈ 800 ns. The output of the (doubled) dye laser (Quanta-Ray PDL-2, pumped by Continuum Minilite II, 10 Hz repetition rate) was ≈ 300 μJ at 583.5 nm and ≈ 100 μJ at 313 nm, both

with a bandwidth of 0.3 cm^{-1}. The LIF optics imaged a 3 mm long probe volume onto the photodetector.

In both setups, we use two identical photomultipliers (Hamamatsu, H7732-10 module with R928 tube), the transients of which were simultaneously recorded using a two-channel digitizer (National Instruments NI PCI-5124, 12-bit, 200 MS/s, 150 MHz for Setup 1 and AlazarTech ATS460, 14-bit, 125 MS/s, 65 MHz for Setup 2). For both our setups, the cavity round-trip times are similar to the laser pulse lengths resulting in a partially time-resolved pulse train exiting the cavity.[24,30] The temporal resolution is not sufficient to observe the remnants of the pulse train due to the signal rise time of the photomultipliers and the bandwidth of the digitizer cards. An example of the smoothed-out transients can be seen in Fig. 2.

C. Data acquisition and analysis

For each laser shot, the LIF transient and the CRD transient were measured simultaneously as shown in Fig. 2 (a) and (b), respectively. The CRD transient follows the typical exponential decay (Fig. 2(b)) from which the ring-down time, τ, is extracted by a non-linear least-squares fit. In combination with the empty-cavity ring-down time, τ_0, the absorption coefficient, α, is determined as
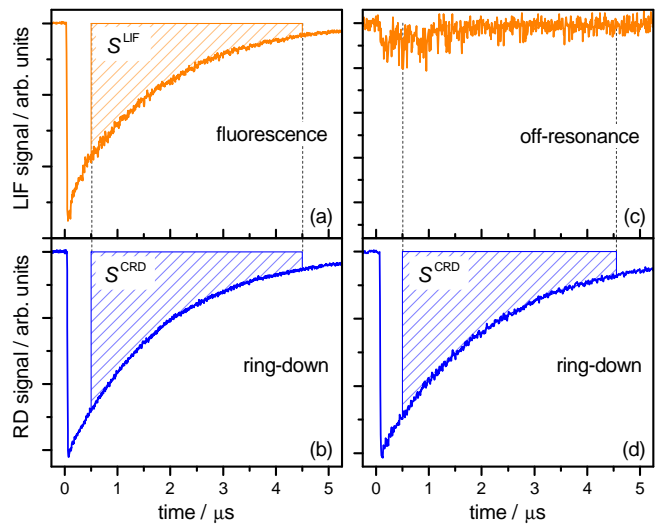
FIG. 2. Simultaneously recorded (a) LIF and (b) CRD transients of jet-cooled BPEB on resonance (vibronic molecular transition at 319.44 nm, see Fig. 4, $\tau = 1.78$ μs). The integration limits used to derive S^{CELIF} are indicated by the hashed areas. Simultaneously recorded (c) broad background absorption (measured with the LIF detector) and (d) CRD transients of jet-cooled BPEB off resonance (321.0 nm, $\tau_0 = 2.10$ μs). The vertical scale in panel (c) is magnified to show the presence of the weak background absorption. The absolute noise is equivalent to the baseline noise in panel (a).

in a typical CRD experiment (Eq. 2).

We also integrate the CRD transient to extract S^{CRD} (*cf.* Eq. 10). The LIF transient, which in this case follows the ring-down decay, is integrated to yield S^{LIF}. According to Eq. 14 the CELIF signal, S^{CELIF}, is obtained through a shot-to-shot normalization of S^{LIF} with respect to S^{CRD}. Details of the fitting and integration procedure are given in the supplementary material.

III. RESULTS

Based on our previous CRD work,[27] we chose BPEB as our model system. One of its characteristic properties is a fluorescence lifetime of < 1 ns following the $S_1 \leftarrow S_0$ electronic excitation.[31] The left column of Fig. 2 shows samples of simultaneously recorded LIF and CRD transients on resonance. As the fluorescence lifetime is negligible compared to the $1-2$ μs ring-down times, the LIF transient follows the exponential decay of the ring-down transient. Based on this fact, we chose the same integration limits for the LIF and CRD transients to derive the normalized CELIF signal (Eq. 14). In the more general case, where the fluorescence lifetime is no longer small in comparison to the ring-down time, both the entire LIF and CRD transients need to be integrated to ensure correct normalization.

In order to assess detection limits and signal-to-noise ratios, we also measured off-resonance transients of BPEB at 321 nm shown in the right column of Fig. 2. BPEB experiences a broad absorption in the $317-321$ nm range that can possibly be attributed to a broad electronic transition or resonance-enhanced scattering.[27] We can detect this weak absorption in a seeded molecular beam (Fig. 2(c)) with our CELIF setup. The corresponding CRD transient (Fig. 2(d)) did not show a reduction in ring-down time with respect to the empty cavity demonstrating the higher sensitivity of CELIF.

We confirmed the validity of the CELIF normalisation according to Eq. 14 by measuring the fluorescence of acetone in a filled cavity. Displayed in Fig. 3(a), the laser intensity, as measured by S^{CRD}, is linearly proportional to the fluorescence signal, S^{LIF}, with the gradient equal to S^{CELIF}. The linear least-squares fits demonstrate the linear correlation between S^{CRD} and S^{LIF} and show the absence of saturation effects.

The linearity of S^{CELIF} with respect to the absorption coefficient (or sample density), Eq. 14 was confirmed using N_2 Rayleigh scattering (Fig. 3(b)). The Rayleigh scattering loss in the filled cavity was simultaneously measured by CELIF and CRD as function of N_2 pressure (determined by a calibrated capacitance manometer). The ratio of the slopes of the linear least-squares fits to both data series was used to determine $\mathcal{K}$ for the absolute cal-
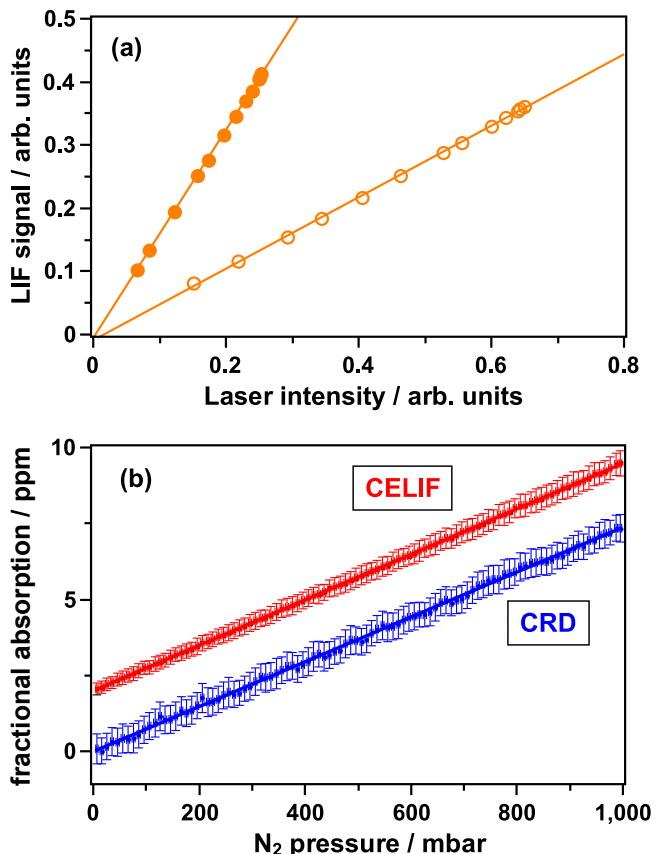
FIG. 3. (a) Detected acetone fluorescence (S^{LIF}) as a function of the incident laser intensity (313 nm) as measured by the integrated ring-down transient (S^{CRD}) at two pressures of 0.1 mbar ($\circ$) and 0.3 mbar ($\bullet$) leading to a fractional absorption per pass of $(1.42 \pm 0.02) \cdot 10^{-3}$ and $(4.31 \pm 0.04) \cdot 10^{-3}$, respectively (linear least-squares fits). Each data point represents the average over 5000 laser shots. The standard errors are significantly smaller than the symbol size. (b) Pressure-dependent N_2 Rayleigh scattering at 583.5 nm. The fractional "absorption" is derived from the ring-down times. Each data point is based on an average of 311 laser shots in a 10 mbar pressure range and the error bars represent the standard deviation. The solid lines are the linear least-squares fits to the data, the slopes of which were used to calibrate the CELIF data (shifted for clarity).

ibration of CELIF data with respect to the CRD measurement. The data analysis is discussed in more detail in the supplementary material.

Fig. 4 shows a series of simultaneously recorded CRD and CELIF spectra of jet-cooled BPEB at different sample densities, analysed using Eqs 2, 14–15. This measurement highlights the capabilities of CELIF with respect to its dynamic range and sensitivity. By contrast, the performance of the CRD measurement in this setup is limited by the small sample volume (diameter of the molecular beam) and the comparatively low reflectivity of the UV cavity mirrors. For the CELIF measurement the gain of the LIF detector was lowered with increasing sam-
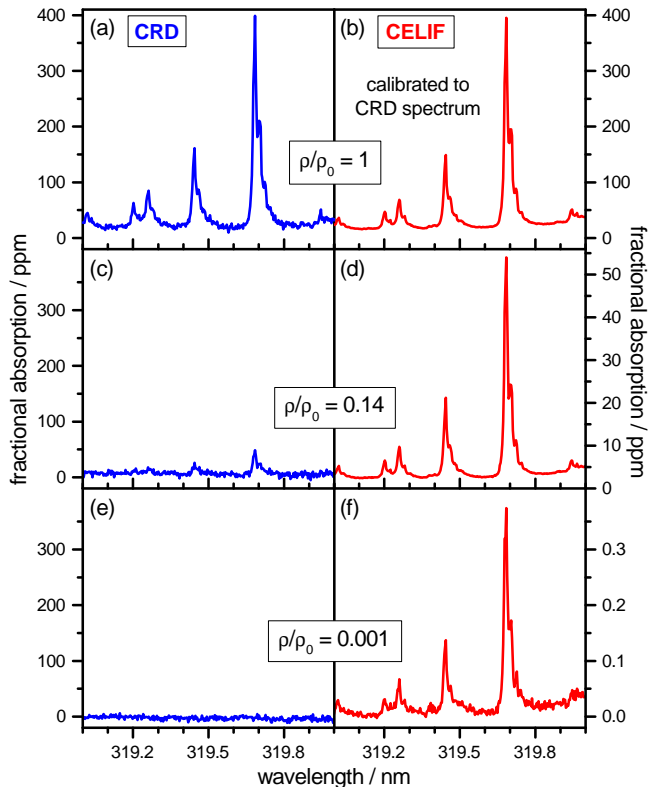
FIG. 4. Comparison of simultaneously recorded CRD (left column) and CELIF (right column) spectra of jet-cooled BPEB with decreasing relative concentrations, ρ/ρ_0. The CRD spectra, (a), (c) and (e), are shown to the same scale as the absolute noise does not change with concentration. The fractional absorption of the CELIF spectrum (b) was calibrated via Eq. 15 based on the simultaneously measured CRD spectrum (a). The CELIF spectra (d) and (f) were calibrated with respect to spectrum (b). A fractional absorption of 400 ppm corresponds to an absorption coefficient of $2 \cdot 10^{-3}$ cm^{-1} for our sample of 2 mm length. The sample density is of the order of 10^{11} cm^{-3} (*cf.* Ref. 29). For details on the BPEB spectroscopy see Ref. 27.

ple density to avoid saturation. Each consecutive density was measured with overlapping high and low PMT voltages to internally calibrate the gain of the LIF detector. We were able to follow the sample density over a range of more than three orders of magnitude. The very low baseline noise in the CELIF measurements is evident in Fig. 4(b) and (d). Even in Fig. 4(f), where the sample density is reduced by three orders of magnitude, the CELIF baseline noise is comparable to the CRD baseline noise at the highest sample concentration, Fig. 4(a).

IV. DISCUSSION

Our work has shown that recorded CELIF signals are linearly related to absorbances derived from ring-down

time measurements. The cavity ring-down part provides the absolute scale for the LIF measurement without the requirement of any external calibration. With this combination of the two techniques, the high sensitivity of LIF greatly extends the accessible dynamic range of CRDS on an absolute scale due to a greatly improved signal-to-noise ratio. The presence of the cavity introduces changes to the LIF technique that we will discuss in Secs IV A–IV E.

A. General characteristics of CELIF measurements

Fundamentally, CELIF is a LIF measurement. The presence of the cavity and the simultaneously recorded CRD transient are used to normalize and calibrate the LIF signal. We discuss the properties of CELIF in comparison to a single-pass LIF measurement and demonstrate the improvements and limitations invoked by the presence of the cavity.

In a single-pass LIF measurement a major source of noise is the stray light created by scattering of the incident laser pulse by the window substrate, by ghosts of the optical elements in the beam path and by surface scattering inside the chamber housing the sample. Large amounts of stray light can saturate the photodetector and lead to considerable dead times after the initial laser pulse. Commonly, baffles, optical filters and/or time gating of the detector are used to suppress or remove stray light. Particularly challenging are the detection of fluorescence signals on the excitation wavelength and if the fluorescence lifetime is of the order of, or shorter than, the laser pulse length. We discuss this in more detail in Sec. IV D.

In CELIF, the cavity invokes stringent conditions on the shape and spectral composition of the laser beam interacting with the sample. Due to the low mirror transmission, the initial light pulse inside the cavity has an intensity several orders of magnitude lower than in a single-pass LIF setup. Consequently, the stray light is reduced by the same fraction such that saturation of the photodetector is avoided. In well designed, aligned and mode-matched cavity setups the incident laser pulse can predominantly be coupled in TEM$_{00}$ modes, leading to a well defined Gaussian beam waist at the center. Parts of the incoming laser pulse composed of high-order transverse modes, *e.g.* from fluctuations of the laser beam profile, will not be efficiently coupled into the cavity and this light disappears after a few round trips. This unwanted "stray-light" part of the LIF transient can easily be removed by time gating without the use of baffles, *etc.* This allows the detection of the whole fluorescence spectrum, including fluorescence on the excitation wavelength. We have demonstrated the successful and very clean detection of light on the excitation wavelength as shown in the Rayleigh scattering measurements in Fig. 3(b).

The mirror reflectivity and cavity length define the longitudinal mode structure supported by the cavity. This means that in CELIF the spectral composition of the light interacting with the sample is invoked by the cavity.[23–26] By contrast, a single-pass LIF measurement uses the full spectrum of the laser. For all the measurements reported in this paper, the excited state lifetimes (or the lifetime of the virtual state for Rayleigh scattering) are significantly shorter than the cavity round-trip times. As a consequence, the linewidths exceed the free spectral range of the cavity multiple times and as such the transitions are in resonance with many cavity modes.

The photon-bullet model used in the derivation in Sec. II A does not take the spectral composition of the light into account. Following Ref. 24, we have confirmed that once the laser bandwidth spans more than 1.5 times the free spectral range of the cavity, the frequency-integrated light intensity entering the cavity is independent of the laser carrier frequency and equals $I_{in}T$, see Eq. 4. Thus, through the repeated use of the light pulse inside the cavity, the integrated light intensity creating the LIF signal in a CELIF experiment is $I_{in}T/(1 - R)$, assuming a small fractional absorption, $\mathcal{L} \ll 1$. In a single-pass, pulsed LIF experiment, the fluorescence signal is created by the full intensity of the probe laser, I_{in}. Therefore, the total light intensity in both techniques differs only by the factor $T/(1 - R)$, *cf.* Eqs 4 and 7. For our setup we conducted a Rayleigh scattering measurement of N_2 in a filled cavity (150 mbar) at a wavelength of 321 nm to determine the factor $T/(1-R)$. Combining Eqs 3, 4 and 7 in the limit of $\mathcal{L} \ll 1$, the transmission of the entrance mirror is given by

$$T = \frac{S^{LIF} \cdot (1 - R)}{I_{in} \cdot \alpha_R \cdot g} . \qquad (16)$$

The light incident on the entrance mirror, I_{in}, was measured with a pyro detector. The measured ring-down times τ_0 and τ are used to obtain $1 - R$ and the Rayleigh scattering coefficient, α_R. The geometric detection efficiency of the LIF assembly was calculated by ray tracing using Monte-Carlo integration. The quantum efficiency and the gain of the PMT to measure S^{LIF} were taken from its data sheet. The latter three quantities combine to the geometry-dependent factor of the detection system, g. From this measurement we obtain $T/(1-R) = 0.4 \pm 0.2$. This value is consistent with the the data for T and R as listed by the manufacturer.[32] Consequently, the light available to invoke S^{LIF} in our CELIF setup is 40% of the light available in an equivalent single-pass LIF measurement. Therefore, in terms of number of photons interacting with the sample, CELIF and single-pass, pulsed LIF are comparable. However, the photon flux per sample pass is several orders of magnitude lower for CELIF which will result in much reduced power broadening of spectral lines.

Compared to a CRD measurement, CELIF can be used over a wider range of wavelengths using the same set of cavity mirrors. The sensitivity of CRD crucially depends on the large effective path length given by the high mirror reflectivity. Following the derivation of Eqs 13 and 14, the CELIF signal is largely independent of the mirror reflectivity and as a consequence the useful wavelength range of the mirrors is extended.

The number of molecules that are excited in any given time interval is proportional to the number of laser photons present in the cavity. Consequently, the time evolution of the LIF signal is the temporal convolution of the ring-down and fluorescence decays. In a typical single-pass LIF experiment using ns laser pulses, the sample can be regarded as static. In CELIF, however, the time resolution is given by the ring-down time. If the sample density changes on the time scale of the ring-down decay, this change needs to be accounted for.[33]

B. Limit of detection and extension of dynamic range

The dynamic range of absorbance measurements is at one end determined by the limit of detection (LOD) defined by the noise level and at the other end by saturation. It is important to note that in CRD measurements the noise level stays almost constant, see Fig. 3(b). The lowest absorbance that can be measured needs to cause a statistically significant change in the ring-down time. At the other end, CRD measurements are not valid any more when large absorbances lead to very short ring-down times. A typical pulsed UV/vis CRD measurement spans two to three orders of magnitude in dynamic range.[34,35]

In a LIF experiment, the LOD is defined by the baseline noise of the detection system. At very low signals, when the photodetector amplification is high, the baseline noise is amplified as well. The absolute noise typically increases with signal as can be seen in the upper trace of Fig. 3(b).

We quantified the limits of detection of the fractional absorptions, $\mathcal{L} = \alpha s$, from simultaneous CELIF and CRD measurements following the recommendations in Ref. 36. The gross analyte signal, S_t, was determined from the strongest absorption at 319.69 nm, *cf.* Fig. 4. The system blank, S_b, was recorded far off resonance at 320.98 nm and comprises the fluctuation in nozzle intensity and the noise of the detection system. Data is recorded as a function of sample density and averaged over 2,500 laser shots. The noise of the system blank is its standard deviation, σ_b. Fig. 5 shows the net signal over the noise, $(S_t - S_b)/\sigma_b$, as a function of the net signal, $S_t - S_b$, for both CELIF and CRDS. The commonly accepted limit of detection of $3\sigma_b$ is indicated by the horizontal line in the plot. Any data point above this line is a detected signal with at least a 99.7% confidence limit. The CRD measurement at 52 ppm with
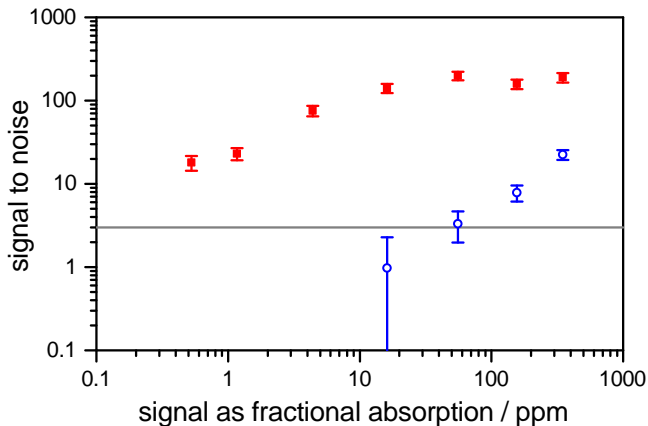
FIG. 5. Comparison of limits of detection (LOD) for CELIF (■) and CRD (○) measurements of jet-cooled BPEB. The signal-to-noise ratio is the baseline-corrected signal (fractional absorption per pass) divided by the standard deviation of the baseline noise (σ_{b}). The error bars are the standard deviations originating from the statistical spreads of the fractional absorptions. The horizontal axis shows the baseline-corrected fractional absorption. The typical LOD of $3\sigma_{\mathrm{b}}$ is indicated by the horizontal line. The data was extracted from simultaneously recorded transients at 319.69 nm (*cf.* Fig. 4).

$(S_{\mathrm{t}} - S_{\mathrm{b}})/\sigma_{\mathrm{b}} = 3$ corresponds to the strongest absorption line in the spectrum shown in Fig. 4(c). This LOD corresponds to a minimum detectable absorption coefficient (MDAC) of $\alpha_{\min}^{\mathrm{CRD}} = 2.6 \cdot 10^{-4}$ cm^{-1}, assuming a uniform density over the sample length of $s = 2$ mm. For comparison, the cavity-length adjusted MDAC would reduce to $6.2 \cdot 10^{-7}$ cm^{-1}, if the cavity could be filled with the sample.

In the CRD measurement, σ_{b} is independent of sample concentration leading to the linear dependence seen in Fig. 5. As in single-pass LIF or CRD measurements, the CELIF signal increases linearly with sample concentration. Due to the broad background absorption of BPEB, in these measurements, the system blank, S_{b}, is proportional to the sample density. This means that at high concentrations, σ_{b} becomes dominated by the shot-to-shot fluctuations in sample density leading to the flattening of the signal-to-noise ratio in Fig. 5.

In our measurements, the accessible range of sample concentrations is limited by the vapor pressure and the temperature control of the sample oven (low concentrations), and the finite sample volume and the thermal stability of the molecule (high concentrations). Higher sample concentrations than shown in Fig. 5 could have been detected by both CELIF and CRDS. Even if the CRD decay is too short to be measured, the fluorescence can be linearly recorded until saturation sets in.

Our lowest CELIF signal-to-noise value of 18 indicates that considerably lower concentrations are accessible. Based on the fluctuations of the signal blank, that is

dominated by the fluctuations in the density of the pulsed molecular beam, we estimate an upper limit of the CELIF LOD of < 0.1 ppm or $\alpha_{\min}^{\mathrm{CELIF}} < 5 \cdot 10^{-7}$ cm^{-1}. For our systems, signal levels were sufficient to analyze integrated LIF transients.

In a separate study, we detected the deuterated mercapto radical (SD) at $\lambda = 323$ nm in a dilute molecular beam using CELIF. The low number density of the radicals in the molecular beam led to a very low number of fluorescence photons which were detected employing photon-counting. In comparison to the BPEB measurements presented here, where the fluorescence signal is derived from integration of transients, photon counting lowered the MDAC to $\alpha_{\min}^{\mathrm{CELIF}} = 7.9 \cdot 10^{-11}$ cm^{-1}.[37] These absorbance measurements on molecular beams demonstrate that CELIF extends the dynamic range by six orders of magnitude in comparison to an equivalent CRD measurement. With the sensitivity of CELIF we were able to measure the absolute sample density of the SD radicals in the molecular beam which was as low as $1.1 \cdot 10^{5}$ cm^{-3}.

C. Sources of noise and error

In this section we focus on the noise and statistical errors of the CELIF measurement and their origins. Figs 4 and 5 clearly show the improvement in quality of CELIF measurements over the associated CRD measurements. We note that shot-to-shot fluctuations in the sample density affect both CRD and CELIF techniques similarly as the same molecules are probed.

A CRD measurement is sensitive to the temporal shape of the ring-down decay. This shape depends on the mode coupling of the laser beam into the cavity, the stability of the mirror alignment and the electronic noise of the detection system. In the UV, additional challenges are the relatively low mirror reflectivity and the lack of stable, narrow-band light sources. A detailed analysis of individual ring-down transients, including statistics of ring-down times, for our setup is presented in the supplementary material.

By contrast, the CELIF signal is not adversely affected by the shape of the LIF and CRD transients as it is derived from the ratio of their integrals, $S^{\mathrm{LIF}}/S^{\mathrm{CRD}}$. The analysis of individual transients showed that S^{LIF} and S^{CRD} can be determined with relative errors on the order of 10^{-4}, see supplementary material. However, for decreasing fluorescence, the noise of the LIF transient will increase, in particular, if the gain of the photodetector is increased. As the noise of S^{CRD} is small and practically constant, the noise of S^{LIF} will determine the noise of S^{CELIF}. At the lowest measured BPEB concentration, we determined a relative error in S^{CELIF} in the order of 2% for individual laser shots. At this concentration, the LIF transients were affected by quantum

noise leading to a low signal-to-noise ratio in S^{LIF}. In this regime, the number of detected photons is still too high for photon-counting due to a large number of co-incidence events, in particular at the start of the decay. However, by decreasing or increasing the amount of incident laser light, the detection can be made suitable for photon counting or integration, respectively.

Fig. 3(b) shows the N_2 Rayleigh scattering measurements comparing CRD and CELIF. In this instance the cavity was filled with N_2 and the pressure was changed slowly. The CRD trace exhibits oscillations with pressure that we attribute to variations in the mirror alignment caused by the pressure gradient across the mirrors. Changes in mirror alignment alter the coupling efficiency of light into the cavity, the temporal profile of the CRD transient and therefore the ring-down time, τ, introducing a systematic error. By contrast, the CELIF trace is unaffected by these variations due to the robust shot-to-shot normalization that automatically compensates for the varying amount of light coupled into the cavity.

In our setup, the mirrors seal the cavity to atmosphere using O-rings, the compression of which is used to align the mirrors. Although we improved our setup in several iterations to reduce the influence of pressure changes, Fig. 3(b) shows that we did not eliminate this systematic error completely for the CRD measurement. Hippler *et al.* have developed a setup entirely immune to pressure variation by moving the mirrors including their alignment mechanics into the sample chamber.[38]

D. Consideration of fluorescence lifetimes

The CELIF method is equally applicable to short and long fluorescence lifetimes compared to the laser pulse length. Short fluorescence lifetimes pose particular challenges for single-pass, pulsed LIF. The fluorescence signal is obscured by the stray light of the excitation pulse and the Rayleigh scattered light from the sample and cannot easily be discriminated against by gated detection. Stray-light-free signal may only be sampled over a limited temporal range leading to a large noise on the digitized signal. Fig. 6 shows the comparison of fluorescence excitation spectra of BPEB, which has a fluorescence lifetime of $\tau_{\mathrm{F}} \approx 500$ ps,[31] obtained with single-pass LIF, from the unnormalized LIF signal with cavity (S^{LIF}) and the normalized CELIF signal (S^{CELIF}). For the single-pass LIF measurement, the laser beam was expanded such that the probe volume was approximately 30 times larger (compared to the measurement with cavity) in order to increase the signal-to-noise ratio and to limit saturation. The single-pass LIF signal was normalized on a shot-to-shot basis against the laser intensity recorded on a pyro detector at the exit window. Stray light was suppressed using a long-pass filter (Semrock, 341 nm blocking edge BrightLine) in front of the LIF
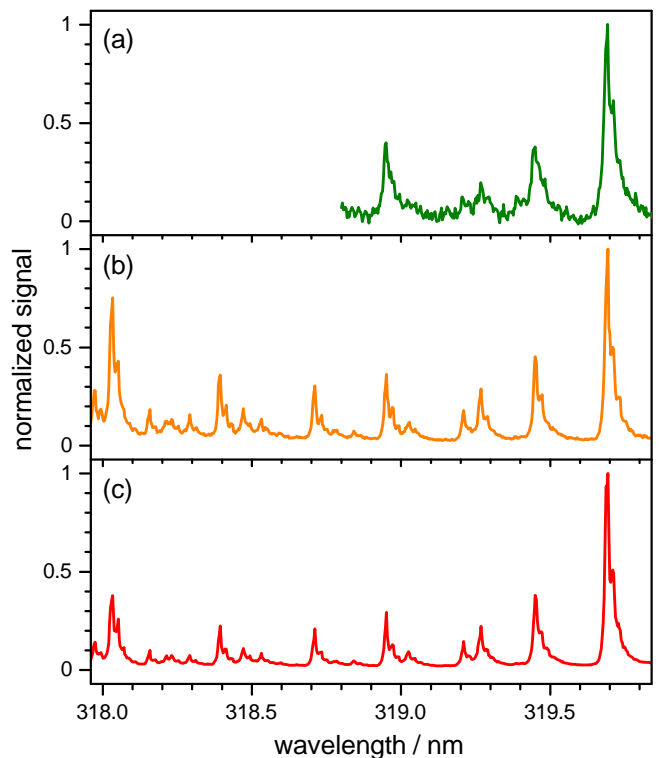
FIG. 6. Comparison of BPEP spectra from (a) single-pass LIF, normalized to the laser intensity, (b) LIF signal with cavity (S^{LIF}), not normalized to the laser intensity, and (c) normalized CELIF ($S^{\mathrm{CELIF}} = S^{\mathrm{LIF}}/S^{\mathrm{CRD}}$). Spectra (b) and (c) are derived from the same scan and only differ by the normalization. Note, the increasing intensities of the peaks at lower wavelengths in (b) compared to (c). The mirror transmission decreases with wavelengths (maximum reflectivity at 330 nm) thus more light is coupled into the cavity at lower wavelengths. The CELIF normalization correctly accounts for this effect.

photomultiplier. Compared to the normalized CELIF spectrum, the observed baseline noise of the single-pass LIF spectrum is approximately 100 times larger whereas for the unnormalized LIF with cavity this reduces to a factor of 6. This demonstrates the difficulty of single-pass LIF to measure the 500 ps fluorescence free from stray light using a 5 ns laser pulse despite the large fluorescence quantum yield of $\Gamma = 0.58$ of BPEB. In order to separate the stray light from fast fluorescence signal, ps lasers and fast signal digitization need to be employed as demonstrated by the fluorescence lifetime measurements of BPEB by Fujiwara *et al.*[31]

With CELIF, we occasionally observe a small initial peak due to light that is not coupled into the cavity (the CELIF equivalent of stray light) at the very start of both the CRD and LIF transients that can be completely removed by appropriate gating. Furthermore, the remaining LIF transient is effectively stretched in time and can be digitized with hundreds of sample points reducing the noise in the recorded LIF signal significantly. This combi-

nation of the suppression of stray light and the low-noise digitization leads to the superior signal-to-noise ratio of CELIF compared to single-pass LIF, in particular for short fluorescence lifetimes. In this case the LIF transient will follow the CRD transient and only a part of the transients needs to be integrated, *e.g.* using the same limits for both the CRD and LIF signals, to ensure the correct CELIF normalization, see Fig. 2. For long fluorescence lifetimes, the only necessary change to gain valid CELIF spectra is the full integration of both transients.

Long ring-down times reduce the number of photons per unit time in the cavity and, if combined with long fluorescence lifetimes, can lead to signal levels that require photon counting.[37] Long fluorescence lifetimes can, in principle, lead to the coherent excitation of the upper state by the pulse train. In CELIF measurements this will rarely lead to saturation effects due to the low photon flux interacting with the sample. However, the user has to ensure that saturation does not invalidate the normalization of the LIF signal.

E. Fluorescence quantum yields

Several groups have used combinations of CRDS with LIF in order to measure quantum yields or quenching rates. Spaanjaars *et al.* combined a CRD measurement with LIF in a single setup, although this was not strictly a single beam experiment as the probe laser was split into two beams that crossed the cylindrical burner at different angles, to extract relative predissociation rates of OH in a flame.[13] The simultaneous measurement of the absorption via CRD and the fluorescence from similar probe volumes allowed an accurate calibration of the relative predissociation rates and quantum yields. Bahrini *et al.* measured absorption and fluorescence excitation spectra of CaBr and CaI with a cavity ring-down setup to obtain relative quantum yields within individual vibrational bands. Unfortunately, it is not clear how the LIF and CRD measurements were calibrated with respect to each other, in particular, as only some spectra were measured concurrently.[15] The experiments by Hagemeister *et al.* deployed a similar experimental approach to the one described here to measure relative fluorescence quantum yields from single vibronic level of tropolone and tropolone-water clusters.[14] However, in order to extract accurate relative quantum yields, knowledge of the wavelength dependent mirror transmission would be required, see Eq. 13.

In the following, we propose how CELIF could be used to measure absolute fluorescence quantum yields in a self-calibration scheme with Rayleigh scattering. Considering Eqs 3 and 13–14, the absorption coefficient is

$$\alpha(\lambda) = \frac{T(\lambda)}{2g \cdot \Gamma(\lambda)} \cdot S^{\mathrm{CELIF}} . \qquad (17)$$

Performing a Rayleigh scattering measurement (where $\Gamma = 1$ by definition) with the CELIF setup, the Rayleigh scattering coefficients, $\alpha_{\mathrm{R}} = \sigma_{\mathrm{R}}\rho$, can be extracted from the simultaneous ring-down time measurement or from known Rayleigh cross sections and sample densities. The fraction $\alpha_{\mathrm{R}}/S_{\mathrm{R}}^{\mathrm{CELIF}}$ is the calibration factor $\mathcal{K}_{\mathrm{R}}(\lambda) = T(\lambda)/2g$. The absolute fluorescence quantum yield, Γ, of the sample molecule is then obtained from a subsequent CELIF measurement using the above calibration,

$$\Gamma(\lambda) = \mathcal{K}_{\mathrm{R}}(\lambda) \cdot \frac{S^{\mathrm{CELIF}}(\lambda)}{\alpha^{\mathrm{CRD}}(\lambda)} , \qquad (18)$$

where the absorption coefficient, α^{CRD}, is determined from the ring-down time measurement. Strictly, the wavelength dependence of g needs to be considered with respect to the spectral response of the detection system (from data sheets) and the fluorescence spectrum.

V. CONCLUSIONS

We have demonstrated how a conventional, pulsed CRD setup can be extended by fluorescence detection in a straightforward manner that combines the advantages of both the CRD and LIF techniques. The CELIF technique uses the same laser beam and sample in the cavity. Its simultaneous absorption (CRD) and fluorescence (LIF) detection allows a rigorous absolute calibration of the LIF measurement at sample densities that lead to a measurable reduction in ring-down time. This calibration can subsequently be applied across the entire LIF dynamic range. From the calibrated CELIF signals, absolute quantities, such as sample densities, absorption cross sections and potentially fluorescence quantum yields, can be extracted. The only additions to a CRD setup are LIF collection optics, a photodetector and a recording channel. In this study, we have shown how the limited dynamic range of the CRD measurement can be extended by at least three orders of magnitude using the combined technique.

We believe that CELIF is most suited for localized sample volumes, such as molecular beams, flames or surfaces. In these situations, CRDS cannot fulfil its full potential due to the small absorption path length, and single-pass LIF may need to be calibrated with much effort to obtain absolute quantities. With CELIF, pulsed and absolute measurements are again possible in the UV-vis spectral region with sensitivities that can approach those of some cavity-enhanced techniques in the IR.

In our respective research areas, we apply CELIF to molecular spectroscopy in supersonic beams and dynamics at surfaces. Other research fields where absolute spectroscopic quantities such as cross sections and quantum yields are required include astrochemistry, atmospheric chemistry, trace-gas detection and plasma

physics/chemistry. In chemical reaction dynamics, using molecular beams or (ultra-)cold molecules, CELIF offers the prospect of measuring absolute densities using modest experimental means, thus allowing the determination of accurate absolute cross sections in scattering experiments.[37]

We believe that CELIF is an elegant, easy to implement and cost effective way to gain these absolute quantities over a large dynamic range and we hope that it finds applications in many research fields.

VI. SUPPLEMENTARY MATERIAL

See supplementary material for more detailed procedures for the data and error analyses.

VII. ACKNOWLEDGEMENTS

[1] H. H. Telle, A. G. Ureña, and R. J. Donovan, *Laser Chemistry* (Wiley, 2007).

[2] J. L. Kinsey, Annu. Rev. Phys. Chem. **28**, 349 (1977).

[3] R. N. Zare, Ann. Rev. Anal. Chem. **5**, 1 (2012).

[4] C. Brecher and L. A. Riseberg, Phys. Rev. B **13**, 81 (1976).

[5] G. Gagliardi and H.-P. Loock, eds., *Cavity-Enhanced Spectroscopy and Sensing* (Springer, 2014).

[6] G. Berden and R. Engeln, eds., *Cavity Ring-down Spectroscopy: Techniques and Applications* (Wiley-Blackwell, 2009).

[7] A. O'Keefe and D. A. G. Deacon, Rev. Sci. Instrum. **59**, 2544 (1988).

[8] A. Pipino, J. Hudgens, and R. Huie, Rev. Sci. Instrum. **68**, 2978 (1997).

[9] L. van der Sneppen, F. Ariese, C. Gooijer, and W. Ubachs, Ann. Rev. Anal. Chem. **2**, 13 (2009).

[10] M. Mazurenka, L. Wilkins, J. V. Macpherson, P. R. Unwin, and S. R. Mackenzie, Anal. Chem. **78**, 6833 (2006).

[11] K. K. Lehmann and H. Huang, "Frontiers of molecular spectroscopy," (Elsevier, 2009) Chap. Optimal Signal Processing in Cavity Ring-Down Spectroscopy, p. 624.

[12] A. Foltynowicz, T. Ban, P. Masłowski, F. Adler, and J. Ye, Physical Review Letters **107**, 233002 (2011).

[13] J. Spaanjaars, J. terMeulen, and G. Meijer, J. Chem. Phys. **107**, 2242 (1997).

[14] F. C. Hagemeister, C. A. Arrington, B. J. Giles, B. Quimpo, L. Zhang, and T. S. Zwier, "Cavity-ringdown spectroscopy," (ACS, 1999) pp. 210–232.

[15] C. Bahrini, S. Douin, J. Rostas, and G. Taieb, Chem. Phys. Lett. **432**, 1 (2006).

[16] D. Tokaryk, A. Adam, and M. Slaney, Chem. Phys. Lett. **433**, 264 (2007).

[17] B. A. Richman, A. A. Kachanov, B. A. Paldus, and A. W. Strawa, Optics Express **13**, 3376 (2005).

[18] C. B. Dreyer, S. M. Spuler, and M. Linne, Combust. Sci. Technol. **171**, 163 (2001).

[19] J. Luque, P. Berg, J. Jeffries, G. Smith, D. Crosley, and J. Scherer, Appl. Phys. B **78**, 93 (2004).

[20] N. Lamoureux, P. Desgroux, A. E. Bakali, and J. Pauwels, Combust Flame **157**, 1929 (2010).

[21] N. H. Nahler, J. D. White, J. LaRue, D. J. Auerbach, and A. M. Wodtke, Science **321**, 1191 (2008).

[22] D. Lee, Y. Yoon, B. Kim, J. Lee, Y. Yoo, and J. Hahn, Appl. Phys. B **74**, 435 (2002).

[23] P. Zalicki and R. N. Zare, J. Chem. Phys. **102**, 2708 (1995).

[24] J. T. Hodges, J. P. Looney, and R. D. vanZee, J. Chem. Phys. **105**, 10278 (1996).

[25] K. K. Lehmann and D. Romanini, J. Chem. Phys. **105**, 10263 (1996).

[26] D. Romanini, I. Ventrillard, G. Méjean, J. Morville, and E. Kerstel, "Cavity-enhanced spectroscopy and sensing," (Springer, 2014) Chap. 1, pp. 1–60.

[27] S. J. Greaves, E. L. Flynn, E. L. Futcher, E. Wrede, D. P. Lydon, P. J. Low, S. R. Rutter, and A. Beeby, J. Phys, Chem. A **110**, 2114 (2006).

[28] A. Beeby, K. Findlay, P. J. Low, and T. B. Marder, J. Am. Chem. Soc. **124**, 8280 (2002).

[29] We estimate an absorption cross section of the strongest vibronic line at 319.69 nm in excess of $5 \cdot 10^{-15}$ cm^2 from the gas-phase UV spectrum of BPEB at 120 °C (Ref. 27). The maximum of the gas-phase spectrum was scaled to match the maximum extinction coefficient of BPEB in cyclohexane solution at room temperature: 58 000 dm^3 mol^{-1} cm^{-1} (Ref. 28). We assume that the cooling in the supersonic expansion increases the population in the vibrational ground state by at least a factor of 100.

[30] M. D. Wheeler, S. M. Newman, A. J. Orr-Ewing, and M. N. R. Ashfold, J. Chem. Soc. Faraday Trans. **94**, 337 (1998).

[31] T. Fujiwara, M. Z. Zgierski, and E. C. Lim, J. Phys, Chem. A **112**, 4736 (2008).

[32] *Layertec Catalog*, Layertec GmbH, Mellingen, Germany (2015), page 115.

[33] S. Brown, A. Ravishankara, and H. Stark, J. Phys. Chem. A **104**, 7044 (2000).

[34] L. Wang and J. Zhang, Environ. Sci. Technol. **34**, 4221 (2000).

[35] J. Lauterbach, D. Kleine, K. Kleinermanns, and P. Hering, Applied Physics B: Lasers and Optics **71**, 873 (2000).

[36] D. MacDougall and W. Crummett, Anal. Chem. **52**, 2242 (1980).

[37] A. Mizouri, L. Z. Deng, J. S. Eardley, N. H. Nahler, E. Wrede, and D. Carty, Phys. Chem. Chem. Phys. **15**, 19575 (2013).

[38] M. Hippler, C. Mohr, K. A. Keen, and E. D. McNaghten, Journal of Chemical Physics **133**, 044308 (2010).